

## Matching Temperature and Conductivity Sensor Response Characteristics

FARHAD M. FOZDAR, GEOFFREY J. PARKER AND JÖRG IMBERGER

Department of Civil Engineering, The University of Western Australia, Nedlands, WA 6009 Australia,

(Manuscript received 27 November 1984, in final form 12 June 1985)

### ABSTRACT

A method to match the response of the SBE-3 temperature sensor and the SBE-4 conductivity cell is described. The technique uses a recursive filter in the time domain, which allows direct calculation of salinity and density, and thus offers a significant computational advantage over other methods. The response of any sensor may be matched or sharpened using this method provided that the sensor can be modeled appropriately.

Using this method the useful bandwidth of the SBE-3 temperature sensor may be improved by a factor of between 3 and 7, depending on the permissible signal-to-noise ratio degradation. It is also possible to match the SBE-3 and SBE-4 responses closely and thus remove spikes in the profiles of calculated salinity and density.

### 1. Introduction

The need to measure temperature, salinity, and density profiles in the field has resulted in the development of sensors that are allowed to free-fall through the water when released from a research vessel. These sensors fall at a constant velocity and sample conductivity, temperature and water pressure. From these measurements, salinity and density may then be calculated (UNESCO, 1981).

The work described in this paper deals with the temperature and conductivity sensors that are used on the conductivity-temperature-depth (CTD) probes developed by the Centre for Environmental Fluid Dynamics (CEFD). These probes use commercially available sensors; specifically a SEA-BIRD SBE3 oceanographic thermometer and a SEA-BIRD SBE-4 conductivity cell. The frequency output from each sensor is transmitted to a counterboard circuit that counts the number of cycles and partial cycles within each 20 ms period with 20 ns (50 MHz) resolution. Thus the sensor provides an average frequency output for each sampling interval. The output is converted to the physical variable through a calibration equation contained in a ROM and evaluated by a microprocessor within the CTD probe. Calibrated data are sent to the research vessel via a signal cable. A full discussion of the CTD probe is given by Fozdar (1983).

The sensing element of the SBE-3 sensor is a glass-coated thermistor bead protected by a 0.8 mm diameter stainless steel tube. The thermistor forms one arm of a Wien bridge oscillator circuit, which converts its resistance to a frequency. The sensor time constant specified by the manufacturer is 70 ms.

The SBE-4 conductivity sensor is a flow-through cell, employing three electrodes in a 0.12-m long, 4-mm

diameter glass tube (see Pederson and Gregg, 1979). The outer electrodes are held at the same potential, and the resistance between the center electrode and the outer pair is measured to yield the conductivity of the fluid within the cell. Thus, the conductivity sensor output represents a spatial average over the length of the cell, and this results in a temporal smoothing that is dependent on flushing time of the cell. Because of the high hydraulic resistance of the cell, its flushing time is insufficient for adequate resolution of finescale features, and consequently a pump is required to draw water through the cell at a velocity comparable to the drop velocity. The pumping rate for CTD drops at 1 m s<sup>-1</sup> was calculated to be 38.5 X 10<sup>-6</sup> m<sup>3</sup> s<sup>-1</sup>.

The phenomenon of salinity and density spiking is well documented and details are given by Home and Toole (1980). The problem occurs because the sensors have different, nonideal, dynamic response functions. The nonideal response causes the temperature and conductivity signals to become mismatched, and thus produces over- or undershoot in the calculated salinity and density. Spiking may be caused by a time lag between the sensors, or by a mismatch in the dynamic response functions of the sensors. The time lag between the sensors may be removed by physically shifting the sensors on the CTD probe. The mismatch in response may be corrected by numerically filtering the temperature and conductivity signals to provide "spike-free" salinity and density values (Fofonoff *et al.*, 1974).

At the same time as spiking is eliminated, it is desirable to sharpen the sensor response in order to provide accurate finescale measurements for computing small-scale fluid properties such as the displacement scale and dissipation (Imberger, 1985).

In this paper a computationally efficient technique is presented that allows the sensor responses to be

matched to eliminate salinity and density spiking, and simultaneously improves the response time of the system.

A number of researchers have developed response-sharpening methods that use spectral techniques to correct the signal. These techniques are carried out in the frequency domain, so the Fourier transform of the raw signal must be taken before the correction may be applied. If time-domain calculations (such as salinity and density) are required, the inverse Fourier transform of the corrected spectrum must be taken to obtain a corrected time series. The computational inefficiency of this technique is its main disadvantage. The main advantage is that any response may be corrected, since no assumptions need be made about the sensor or its model. Furthermore, it is possible to achieve more accurate corrections since one can use the actual transfer function of the sensor rather than an approximation.

One example of the frequency-domain technique is given by Caldwell and Dillon (1981), who improved a thermistor response by correcting its spectrum. However the correction applied was that for a first-order filter; the recursive method described herein is more efficient since it can achieve the same correction without converting to frequency. Gregg and Hess (1985) used Legendre polynomials to accurately approximate the transfer function of a sensor in frequency space. The correction must be applied by multiplying the spectrum of the required data by the inverse of the approximated transfer function. It would also be possible to use the actual transfer function and not go through the exercise of polynomial fitting.

Horne and Toole (1980) note that a time-domain correction is preferable to frequency techniques since it allows direct correction of the time series. Their particular method used convolution to correct the signal; the convolution used the inverse Fourier transform of the inverse of the actual sensor transfer function. In essence, their technique is identical to the frequency-domain corrections mentioned previously since convolution in the time domain is equivalent to multiplication in the frequency domain. In fact it can be more efficient to carry out a convolution by taking FFTs of both series and multiplying in the frequency domain. This is due to the comparative efficiency of the FFT algorithm. Hence their method offers no real advantage over spectral techniques.

Fofonoff *et al.* (1974) developed a correction method similar to that presented in this paper. The sensor was modeled as a first-order system described by the differential equation:

$$\frac{dT}{dt} = \frac{1}{\tau} (T_0 - T), \quad (1.1)$$

where  $T_0$  is actual temperature,  $T$  the measured temperature, and  $\tau$  the time constant. They then approximated  $dT/dt$  by taking a least-squares fit to the slope of the time series over 3 points. This has an averaging

effect, which produces good correction at low frequencies but does not correct high frequencies. The result gives a signal-to-noise ratio advantage over the "ideal" correction, however the cutoff frequency is not controllable. The recursive time series technique described in the current paper allows better control over the correction than that used by Fofonoff *et al.* (1974), since sharpening and smoothing occur independently but simultaneously. Furthermore, the least-squares technique requires more calculations than the recursive filtering technique.

## 2. The experiment

In order to properly model the boundary layer around the sensors and reproduce any averaging effects, the experiment needed to be dynamic, with a known input to the sensors. Possible inputs included an impulse or a step. Both of these lend themselves to analysis in the time domain, and it can be shown that a first-order response to either of these inputs has an easily derived transfer function that may be used to design numerical filters. Gregg and Meagher (1980) used a thin heated plume as an impulse input when studying the response of small glass-rod thermistors, but they pointed out that difficulties arose because of temperature changes outside the plume caused by circulation patterns. In the experiment described in the current paper, a step was chosen as the input to the sensors because circulation could be minimized by using a sliding gate as a partition. Furthermore, a step was relatively simple to generate on the large scale required by the dimensions of the SBE sensors.

The University of Western Australia Hydraulics Laboratory concrete flume and towing carriage were used for the experiments. The flume is 50 m long and 1.2 m wide, and the water was at a depth of 1 m. A pneumatically operated gate was placed in the flume to provide the partition for the step interface. The water on one side of the gate was heated and salted to provide the step input. The experimental setup is shown schematically in Fig. 1. The carriage was used to tow the CTD probe through the water with the sensors mounted horizontally, simulating the situation in the field where the CTD probe falls vertically.

A fast-response thermistor and a fast-response conductivity cell were mounted on the carriage to document the interface width and shape remaining behind the retreating gate. The fast-response temperature sensor was a FP-07 thermistor, and the fast-response conductivity (FRC) sensor was a miniature four-electrode cell designed by Head (1983). The fast-response sensors were calibrated *in situ* using temperature and conductivity measurements obtained from the SBE sensors.

The interface was required to be sharp and well defined. It was decided to use a "positive" step, which had an increase in conductivity ( $\sigma$ ) and temperature ( $T$ ), with the salinity and density increasing slight@

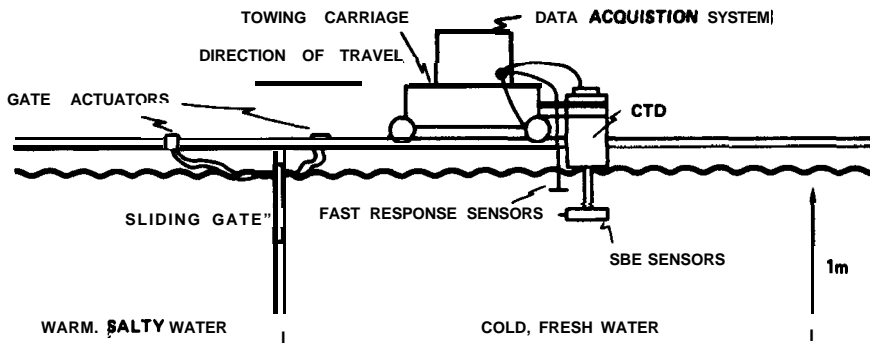


FIG. 1. Schematic elevation view of experimental setup.

across the step. The cold side consisted of tap water ( $\sigma = 0.04 \text{ S m}^{-1}$ ) which remained at room temperature (around  $19^\circ\text{C}$ ). The warm section of the flume was heated to between 2 and  $3^\circ\text{C}$  above room temperature using electric heating elements, and was salted using swimming pool grade salt consisting of 99.4% sodium chloride. The water was stirred before each run to eliminate errors from leakage around the gate, heat diffusion through the gate, and convection of fresh water through the gate during the short interval when the sliding door was open.

For the purpose of finding the transfer functions of the sensors, the interface was assumed to be a perfect step. This assumption was not strictly correct because the opening of the gate caused some mixing of the interface before the CTD sensors passed through; however, the fast-response sensors showed that this mixing was minimal.

### 3. Filtering

Using the stepresponse measurements it is possible to find the sensor time constants. The technique used to determine the sensor time constant from natural logarithmic plots of the normalized step response was as follows.

The analysis presented below is for a first-order system, but may be extended to cover a system consisting of several cascaded first-order stages.

The form of a first-order step response is given by

$$y_k = (y_F - y_I)(1 - e^{-t/\tau}) + y_I, \quad (3.1)$$

where

$y_k$  is the sensor output for sample number  $k$  after the step,

$y_I, y_F$  are the initial and final equilibrium sensor output &

$\tau$  is the time constant of the response (first order),

$t$  is the time from the step ( $=k\Delta$ ),

$\Delta$  is the sampling interval.

This equation is equivalent to the differential equation ( 1.1) used by Fofonoff et al. ( 1974) to model the

sensor. Rearranging (3.1) and taking the natural logarithm of each side yields

$$\frac{-1}{\tau} = \frac{\ln y'_k}{t}, \quad (3.2)$$

where

$$y'_k = \frac{y_F - y_k}{y_F - y_I}$$

Thus, the slope of a plot of  $\ln y'_k$  versus time is equal to  $-1/\tau$ . A plot in this form also gives an indication as to whether or not the response of a sensor is first-order. The dominant time constant is measured as long after the step as possible to remove the effects of shorter time constants. These may be subsequently removed.

During the sampling process the continuous signal is captured at instants  $k\Delta$  separated by the sampling interval  $\Delta$ . This produces samples  $S_k$  where  $S_k = S(k\Delta)$  and  $k$  is an integer. The sequence of samples  $S = S_0, S_1, S_2, \dots, S_k, \dots$  is for convenience written as  $\{S_k\}$ .

The Z-transform of a sequence  $\{S_k\}$  is denoted by  $S(z)$  and is defined as follows:

$$S(z) = \sum_{k=-\infty}^{\infty} S_k z^k, \quad (3.3)$$

where  $z$  is a complex variable in a region of convergence such that  $\sum_k |S_k z^k|$  exists (see Gabel and Roberts, 1973).

It may be assumed that the signal has a value of zero for negative time, allowing the Z-transform to be re-defined by

$$S(z) = \sum_{k=0}^{\infty} S_k z^k. \quad (3.4)$$

The Z-transform has the useful property that a shift in the time domain corresponds to a **premultiplication** by  $z$  in the transform domain. Thus multiplying a sequence by  $z$  has the effect of shifting the time sequence by one sampling interval. Similar analogies with **Fou-**

tier-transform theory exist for convolution. If  $\{S_k\}$  and  $S(z)$ ,  $\{R_k\}$  and  $R(z)$ ,  $\{H_k\}$  and  $H(z)$ , are Z-transform pairs, then

$$S_k = R_k * H_k \Leftrightarrow S(z) = R(z) \cdot H(z), \quad (3.5)$$

where the asterisk denotes convolution, and the dot denotes multiplication. Thus convolution in the time (or sequence) domain corresponds to multiplication in the Z-transform space.

A sensor can be modeled as a filter with a transfer function  $H(z)$ . Thus an input sequence  $X(z)$  produces an output  $Y(z) = X(z) \cdot H(z)$ . The basic method involved in correcting for a sensor response is to find the transfer function  $H(z)$ , invert it to find the inverse transfer function  $H^{-1}(z)$ , and apply it to the output sequence  $Y(z)$  to reproduce the true input  $X(z)$ :

$$X(z) = Y(z) \cdot H^{-1}(z) = X(z) \cdot H(z) \cdot H^{-1}(z). \quad (3.6)$$

The transfer function  $H(z)$  may be found if expressions for the input  $X(z)$  and corresponding output  $Y(z)$  are known:

$$H(z) = \frac{Y(z)}{X(z)}. \quad (3.7)$$

The following analysis will proceed with the **assumption** that the sensor has a first-order response. Thus for an applied stepinput sequence the output is a **first-order exponential** sequence with time constant  $T$ , as shown in Fig. 2. For a step input,

$$x_k = \begin{cases} 0, & \text{for } k < 0 \\ 1, & \text{for } k \geq 0 \end{cases} \quad (3.8)$$

and the exponential output sequence is

$$y_k = \begin{cases} 0, & \text{for } k < 0 \\ 1 - a^k, & \text{for } k \geq 0 \end{cases} \quad (3.9)$$

where  $a = e^{-\Delta/\tau}$ . SHARPEN

The Z-transform of each of these sequences may be found by using the definition (3.4):

$$X(z) = \sum_{k=0}^{\infty} x_k z^k = \sum_{k=0}^{\infty} z^k = \frac{1}{1-z}, \quad |z| < 1 \quad (3.10)$$

$$Y(z) = \frac{(1-a)z}{(1-z)(1-az)}, \quad |z| < 1. \quad (3.11)$$

The first-order transfer function is calculated from (3.7):

$$H(z) = \frac{Y(z)}{X(z)} = \frac{(1-a)z}{(1-z)(1-az)} \cdot (1-z) = \frac{(1-a)z}{1-az}. \quad (3.12)$$

Equation (3.12) is the general transfer function of a first-order system and may be used to find the output sequence for any input sequence. This result can be shown to satisfy the difference equation corresponding to (1.1).

The inverse transfer function allows the reconstruction of the input signal from the sensor output. In terms of the frequency spectrum of the signal, this corresponds to the amplification of the high-frequency components to recover the signal lost by the forward transfer function. Unfortunately, the process also increases any noise present, as shown diagrammatically in Fig. 3a.

In order to reduce the high-frequency noise it is **necessary** to refilter the sharpened signal. If the time constant for the smoothing is chosen to be equal to that of the original sensor, the result will be the original output spectrum. By choosing a smaller time constant (i.e., higher cutoff frequency) for the smoothing a compromise is made between recovering the input perfectly while amplifying noise excessively, and controlling the noise while still retaining a close approximation to the actual input (Fig. 3b).

A first-order filter of the same form derived for the original sensor (3.12) may be used for controlled smoothing. The new time constant is denoted  $\tau'$ , and

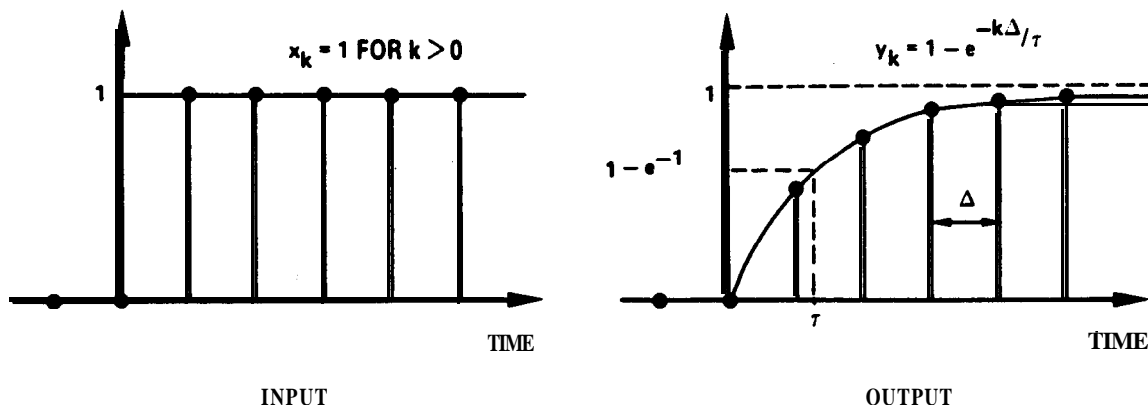


FIG. 2. Input step and output exponential for a first-order system.

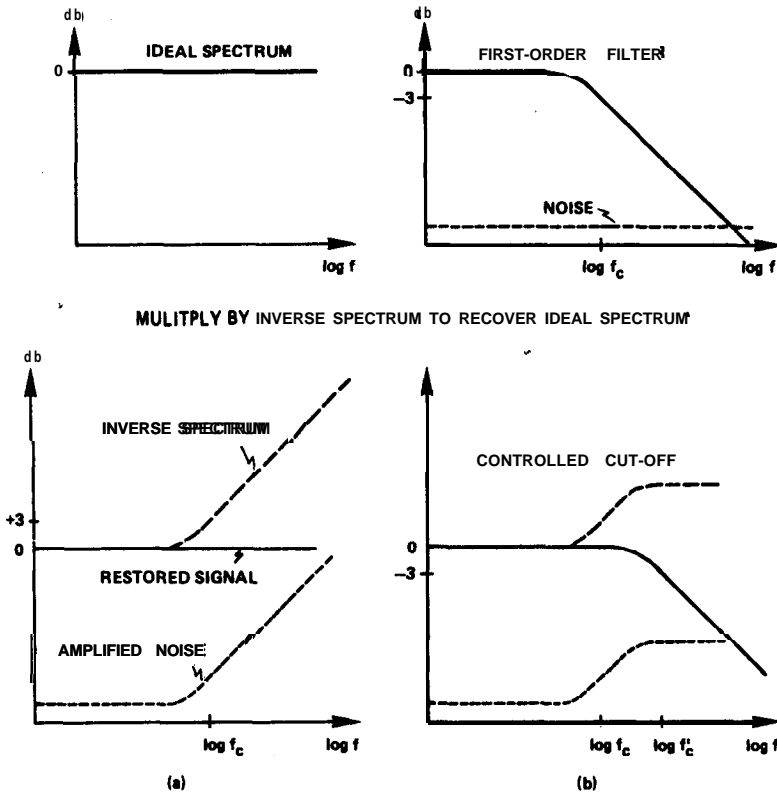


FIG. 3. The effect of multiplying a signal by its inverse spectrum. (a) "Ideal" correction, showing excessive noise amplification; (b) Controlled cut-off of correction at  $f'_c$  to improve signal without excessive noise amplification. Signal (solid line), inverse spectrum (longdashed line), noise (short-dashed line).

results in a total sharpening/smoothing transfer function:

$$\begin{aligned}
 F(z) &= H^{-1}(z) \cdot H'(z) \\
 &= \frac{1 - a'}{1 - a} \cdot \frac{1 - az}{1 - a'z} \quad (3.13)
 \end{aligned}$$

where

$$a' = e^{-\Delta t / \tau'}$$

The separate effects of sharpening and smoothing are shown diagrammatically in Fig. 4. It is possible to cascade several stages of first-order sharpening/smoothing filters to correct sensors that have a response containing several first-order time constants.

The Z-transform representation of the required sharpening/smoothing filter must be transformed back to sequence space for implementation. This is easily accomplished using the shifting property of the Z-transform. Suppose the sharpened/smoothed output sequence is denoted by  $\{R_k\}$ , and the original sensor output by  $\{S_k\}$ .

$$R(z) = S(z) \cdot F(z) \quad (3.14)$$

Substituting (3.13), using the shifting property of the Z-transform, and rearranging gives

$$R_k = \frac{1 - a'}{1 - a} (S_k - aS_{k-1}) + a'R_{k-1} \quad (3.15)$$

Equation (3.15) fully defines the  $k$ th sharpened/smoothed output  $R_k$  in terms of its previous value  $R_{k-1}$  and the sensor output signal  $\{S_k\}$ . The algorithm used to implement this calculation is straightforward.

Cascaded stages of the preceding filter are implemented in the same way, but require more **previous**

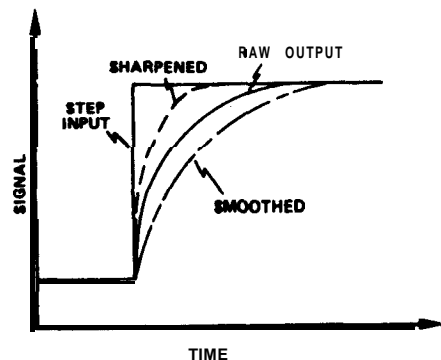


FIG. 4. Sharpening and smoothing of a nonideal step response.

TABLE 1. Summary of data.

Run	Initial temperature (°C)	Final temperature (°C)	Initial conductivity (S m <sup>-1</sup> )	Final conductivity (S m <sup>-1</sup> )	Remarks
1	—	—	0.0395	0.1768	No temperature step, FRC not installed
2	18.203	19.209	0.0405	0.1730	FP-07 not installed
3	18.835	21.489	0.0432	0.1799	Step not sharp
4	18.928	21.023	0.0422	0.1770	
5					
6	19.64 19.53	21.56 21.82	0.0426 0.0454	0.1800 0.1863	

inputs and outputs for the calculation. For example, a filter consisting of three cascaded first-order sharpening/smoothing stages requires the present input (sensor output) and three previous inputs and outputs ( $S_k, S_{k-1}, S_{k-2}, S_{k-3}, R_{k-1}, R_{k-2}, R_{k-3}$ ).

A first-order sharpening/smoothing filter has notation of the form 70/10, which means it was sharpened with a time constant of 70 ms and smoothed with a time constant of 10 ms. A third-order sharpening/smoothing filter has the notation 70/10:50/10:20/10, which is simply a cascade of three first-order filters. A time constant of zero implies that the signal was left unaltered. To further reduce noise at high frequencies, a recursive third-order bilinear Butterworth filter (hereafter referred to as a "brick-wall" filter) was implemented (Gabel and Roberts, 1973). The filter is designated by its 3 dB cutoff frequency (Hz).

4. Results

The dataset described in the following sections consists of six runs through the step. In all runs, the CTD probe velocity was 1.0 m s<sup>-1</sup>, and the sampling frequency was 50 Hz. The conductivity cell was pumped so that the velocity at the cell entrance was equal to the towing speed. The data runs are summarized in Table 1.

The time constants were found from the natural logarithm of the normalized step response (3.2). Once the first time constant was chosen, the process was repeated to correct for further time constants in the sensor response function until the frequency corresponding to the width of the front was reached.

TABLE 2. Time constants (ms) measured from normalized natural logarithmic plots of each raw signal and the sharpened temperature signals.

Run	FRC	SBE-4	FP-07	SBE-3	SBE3	
					67/0	67/0:24/0
1		29	—	—	—	—
2	5.7	21	—	71	25	—
3	5.3	34	13.0	69	24	9
4	5.3	22	12.6	69	24	10
5	5.3	31	15.2	67	23	12
6	4.5	22	12.3	71	27	10

a. Conductivity

The above procedure was carried out on both the SBE-4 and the fast-response sensor. The resulting time constants are shown in Table 2, in which it can be seen that the time constant of the FRC was approximately 5 ms in all runs. This indicates that the step was indeed sharp. Typical FRC and pumped SBE-4 step responses are shown in Fig. 5. An unpumped SBE-4 step response is overlaid for comparison.

The pumped SBE-4 response was sharpened using a first-order sharpening filter with a time constant of 20 ms. Figure 6 shows an example of a corrected output, as well as illustrating the overshoot induced when a time constant of 25 ms was used. A logarithmic plot of the same raw signal is shown in Fig. 7. The short straight-line portion of this curve partly confirms the 20-ms time constant. However, beyond the initial straight-line section of the curve there is a long tail indicating that a first-order model is not a good approximation. Further insight into the behavior of the SBE-4 may be gained by noting the static response of a three-electrode cell to a sharp step change in conductivity moving through the cell.

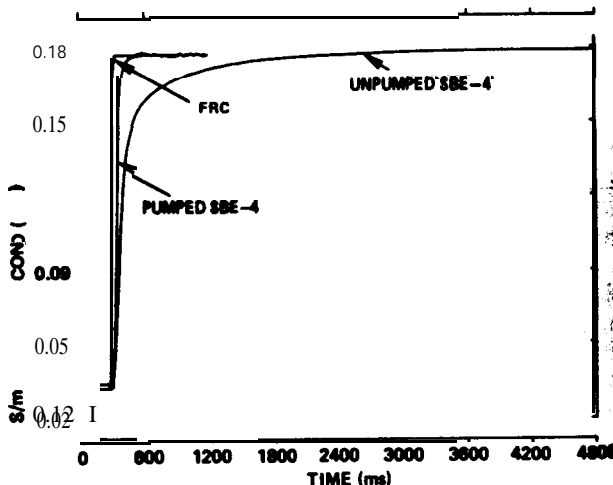


FIG. 5. Conductivity step response measured for FRC cell and pumped SBE-4 sensor (Run 4), with an unpumped response overlaid.

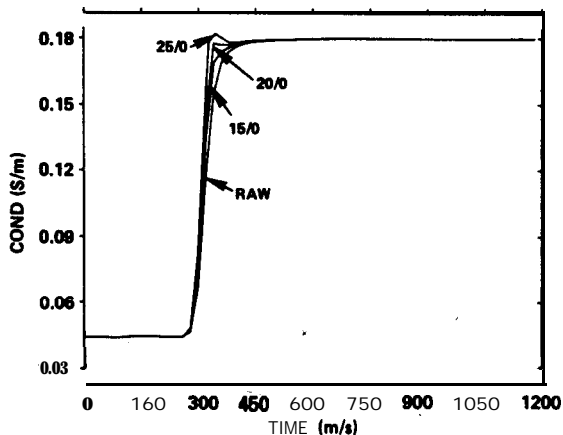


FIG. 6. Raw and filtered conductivity step response for various sharpening filter time constants. Note the overshoot when the time constant is too large.

It may be shown that the conductance (Siemens) measured by the cell is given by:

$$G = \begin{cases} \frac{2a}{L} \left( \frac{C_1 C_2}{C_1(1-k) + C_2 k} + C_2 \right), & 0 \leq k \leq 1 \\ \frac{2a}{L} \left( \frac{C_1 C_2}{C_1(2-k) + C_2(1-k)} + C_1 \right), & 1 \leq k \leq 2 \end{cases} \quad (4.1)$$

where  $L$  is the length of the cell,  $a$  is the cross-sectional area of the cell,  $k/2$  is the fraction of the cell filled with the more conductive fluid, and  $C_1$  and  $C_2$  are the conductivities of the two fluids ( $S\ m^{-1}$ ). Note that this equation is nonlinear. Figure 8a shows plots of the theoretical static response of the conductivity cell calculated from (4.1) for a relatively small conductivity step ( $C_1 = 0.04\ S\ m^{-1}$ ,  $C_2 = 0.17\ S\ m^{-1}$ ) and for a relatively large conductivity step ( $C_1 = 0.031\ S\ m^{-1}$ ,  $C_2 = 4.36\ S\ m^{-1}$ ).

A significant feature of both plots is the "notch" that occurs when the conductivity step is at the midpoint of the cell. Experimental results with the actual cell may be expected to show significant rounding of the theoretical sharp edges and notch because of the finite size of the electrodes and distortion of the electric field in the cell. In addition, mixing of the two solutions within the cell would be expected to produce a wider interface instead of the sharp theoretical input step, resulting in further smoothing of the measured output signal.

For the purposes of the static experiment, the SBE-4 conductivity sensor was removed from the probe and mounted vertically in a 300-mm deep tank. Initially the tank was half filled with tap water ( $\sigma = 0.031\ S\ m^{-1}$ ) so that the cell was completely immersed. Salty water ( $\sigma = 4.36\ S\ m^{-1}$ ) was then injected into the bottom of the tank through a small hole covered by a flat

plate. The water level was slowly raised and the salt water interface moved upwards through the cell. The interface was observed by means of a shadowgraph, and its height was measured on the side of the tank. Readings were taken approximately every 10 mm. These height readings were considered to be accurate to  $\pm 5$  mm. Before each reading the salt water input was turned off and the interface allowed to settle. The conductivity readings were displayed every second and were seen to be constant to within  $0.005\ S\ m^{-1}$ . This procedure was followed until the interface was above the top of the cell and the cell was completely immersed in the salty water. Figure 8b shows a graph of the readings, as well as the position of the electrodes within the cell. It can be seen that the actual response showed the same characteristics as those predicted by the theoretical model.

Although useful in the understanding of the conductivity cell, the static response does not fully define the dynamic response. In the dynamic case there is a great deal of mixing in the cell resulting from the contraction at the entrance, and further mixing occurs because of the recesses in which the electrodes are housed. Modeling the cell as a 4 mm pipe, for a velocity of  $1\ m\ s^{-1}$  entering the 7 mm entrance tube, the velocity in the cell pipe is approximately  $3\ m\ s^{-1}$ , giving a Reynolds number of 12 000. Thus the flow in the cell is turbulent during dynamic conditions. Even if one assumes that the interface moves unaltered through the cell, the total time taken for the step to travel between the outer electrodes would be 37 ms. At a sampling rate of 50 Hz, 37 ms is less than 2 samples, so the shape of the static response curve will not be evident in the dynamic case.

In the dynamic case, a boundary layer exists at the wall of the cell. A delay in mixing through this layer

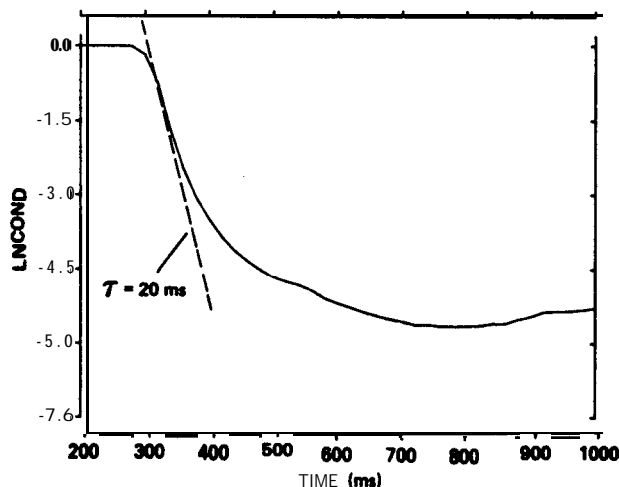


FIG. 7. Natural logarithm of normalized step response for pumped SBE-4 conductivity sensor. The 20 ms slope line is shown for comparison.

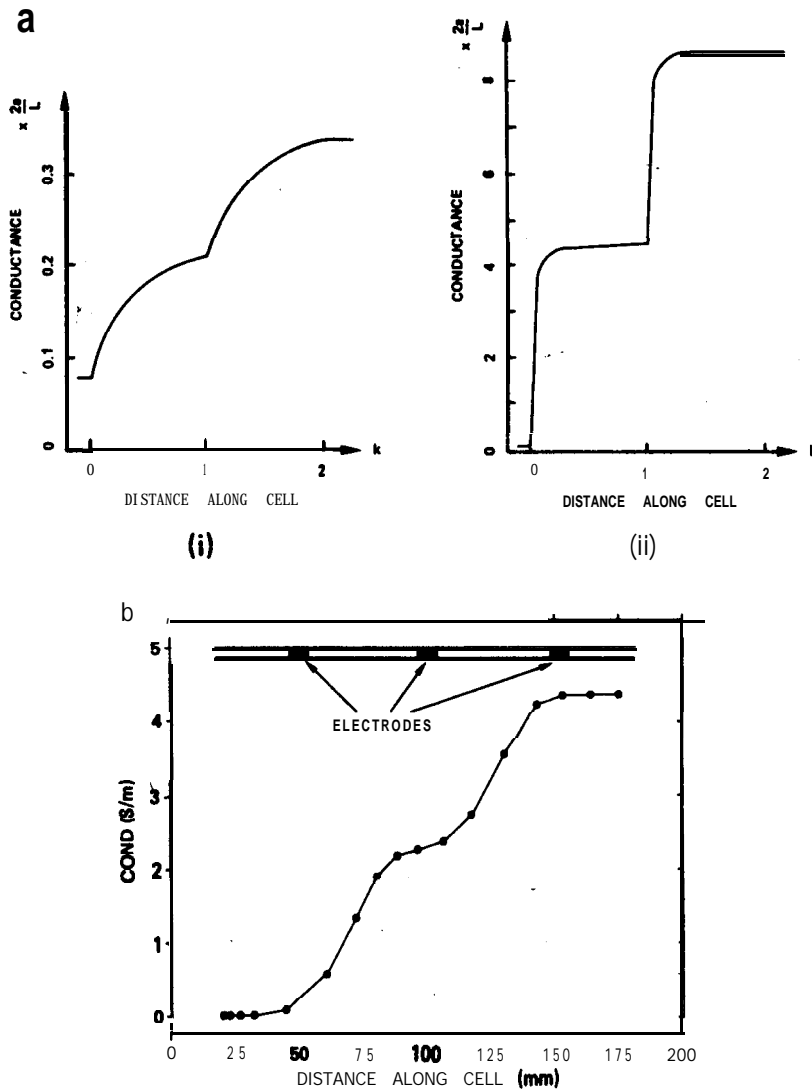


FIG. 8. (a) Theoretical static response of a three electrode cell, and (b) measured static response of SBE-4 sensor.

causes a delay in the conductivity readings reaching equilibrium, because each electrode is in the form of a collar surrounding the cell tube. The boundary layer has been studied by Gregg *et al.* (1982) for a square cross-section conductivity cell. Using numerical models and flow visualization techniques, these authors found that the boundary layer considerably slowed the step response of a cell. This effect will be evident in the SBE-4, even though the SBE cell has a circular cross section which tends to offer less resistance to the incoming flow than does a square cross section.

### b. Temperature

The response of the SBE-3 temperature sensor was slower than that of the pumped SBE-4 conductivity sensor. The time constants measured for the SBE3

sensor and the FE-07 thermistor are shown in Table 2. Note that the FE-07 thermistor had a time constant of around 13 ms, probably due to its thermal inertia, since the FRC gave 5 ms for the step.

The dominant time constant of the SBE-3 sensor was 67 ms, determined by measuring the slope of the natural logarithmic plot of the normalized step response (Fig 9a). Observation of the sharpened signal confirmed this result; larger time constants introduced overshoot (Fig 10a). The logarithmic plot of the sharpened signal is shown in Fig 9b in which a 24 ms time constant is evident. A logarithmic plot of the double-filtered signal revealed a further time constant of 8 ms (Fig. 9c). At this level of filtering, the resolution of the experiment was reached. The fully sharpened signal 67/0:24/0:8/0 is shown in Fig. 10b.

It is hypothesized that these three time constants are

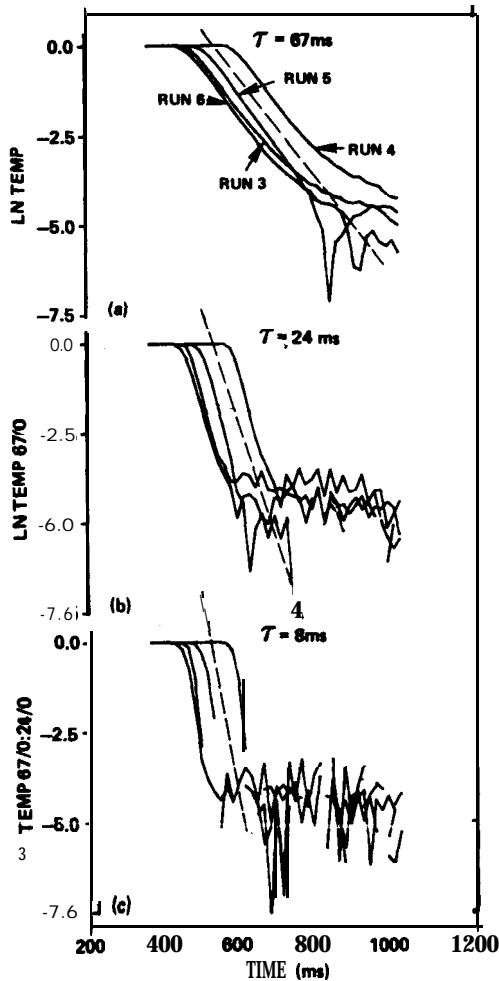


FIG. 9. Natural logarithm of normalized step response for, (a) SBE-3 raw signal, (b) SBE-3 sharpened with a 67 ms time constant, and (c) SBE-3 sharpened with a 67 ms and then a 24 ms time constant. The 67, 24, and 8 ms slopes are shown in the respective figures.

related to the heating of the metal shroud surrounding the thermistor, heating of the actual thermistor, and the exchange of heat through the fluid boundary layer surrounding the sensor. The size of the boundary layer would be dependent upon the speed of the sensor through the water. The speed dependence of the dynamic response of simple glass-rod thermistors is discussed by Gregg and Meagher (1980), who found that the attenuation of the temperature signal by the boundary layer had a significant effect on the response of the thermistor.

### 5. Matching the responses

The purpose of sharpening was to obtain as much high-frequency information as possible. However, there is little value in sharpening the response of each sensor unless the responses can be matched to eliminate spik-

ing. Initially, it was hoped to match the response of the sensors at a sharpness very close to that of the fast-response sensors. Attempts to achieve this were successful in that a sharp "spike-free" signal could be obtained, but problems arose because the filters greatly amplified any noise present in the raw signal. An example is given in Fig. 11, which shows a plot of sharpened temperature (67/0:24/0:8/0), sharpened conductivity (20/0), and the corresponding calculated salinity and density values. Close examination of this dataset reveals fluctuations in the calculated density which were due to noise in the sharpened temperature. This noise was due to the triple cascade filter, and even after filtering the signals with a 12.5 Hz "brick-wall" low-pass filter, some noise was still present.

For this reason, it was decided to match the responses at a level less sharp than the ideal level. This was a compromise between getting the sharpest possible signal and keeping the noise amplification low. It was found that the optimum result was achieved with a 67/10 first-order sharpening/smoothing filter applied to the temperature signal, and a 0/15 sharpening/smoothing filter applied to the conductivity signal.

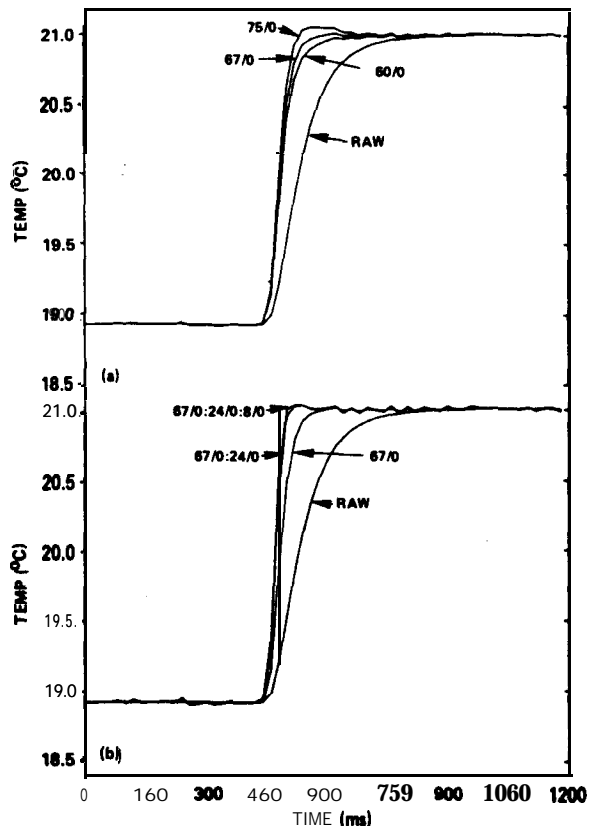


FIG. 10. (a) Raw and filtered temperature step response for various sharpening filter time constants, showing overshoot for time constants greater than 67 ms, and (b) raw and fully sharpened temperature showing each cascade of the sharpening filter.

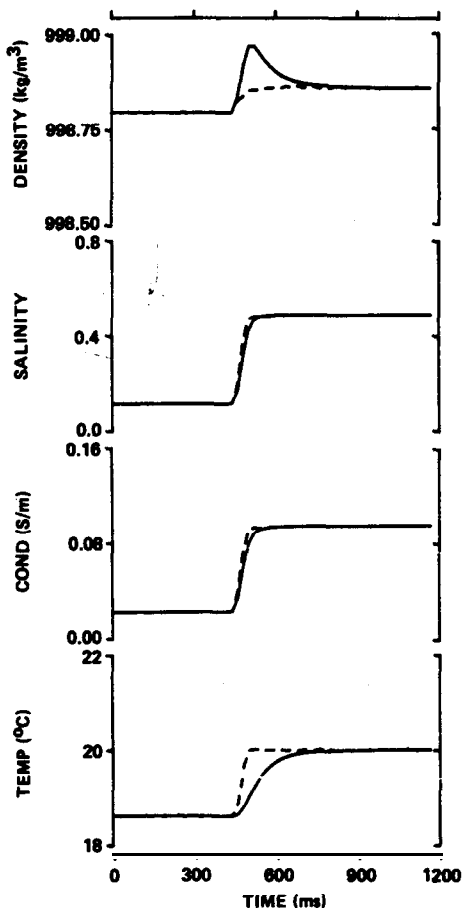


FIG. 1 I. Raw and fully sharpened step response (Run 4), showing the salinity and density calculated from the time series. The SBE-3 temperature has been filtered 67/0:24/0:8/0, and the SBE-4 conductivity filtered 20/0. The practical salinity and density were calculated according to UNESCO (1981).

These filter values were confirmed by the spectral analysis discussed later. Using these time constants, the calculated salinity and density were spike free, and after applying a 12.5 Hz brick-wall low-pass filter to the salinity, density, and sharpened temperature signals they were considered adequately low in noise. For example, typical noise in a raw temperature signal is  $0.0008^{\circ}\text{C}$  rms. Optimum sharpening amplifies this to  $0.0036^{\circ}\text{C}$  rms, and a 12.5 Hz brick wall filter then reduces the noise to  $0.0016^{\circ}\text{C}$  rms. Figure 12 shows a comparison between raw values and optimum values of temperature, conductivity, and density for a typical run.

When implementing the filters it was found that the brick-wall low-pass filter was best applied after the calculation of salinity and density. If the calculations were performed using the brick-walled temperature, the match was not so good because of the nonlinearity of the equation of state for seawater.

It has been shown that the optimum match between temperature and conductivity involved smoothing the

raw conductivity signal since the first-order sharpened temperature was still less sharp than the raw pumped conductivity. Despite the resulting loss of some high-frequency conductivity information, Fig. 12 shows that the optimum density had reached within 10% of its final value in less than 100 ms. The raw density contained a large spike and took over 300 ms for this same response.

## 6. Spectral verification of response matching technique

The signal corrections described in this paper may be further substantiated by considering the signal spectra. Frequency plots of the raw temperature and conductivity impulse-response signals are shown in Fig. 13. It is clear that the mismatch in response was the cause of the spiking evident in the calculated salinity and density. Also shown in Fig. 13 is a spectral plot of the triple time-constant sharpened temperature signal. The 3dB bandwidth has been increased by a factor of about 7, and an increase in the high-frequency noise is also apparent. The flatness of the corrected spectrum is an indication that the cascaded first-order model is an excellent approximation to the actual transfer function of the SBE-3 sensor.

Figure 14 shows the response-matching ability of this technique. The optimum sharpened/smoothed temperature and conductivity signals produce spectra that are matched to within 1 dB from DC to 15 Hz. This

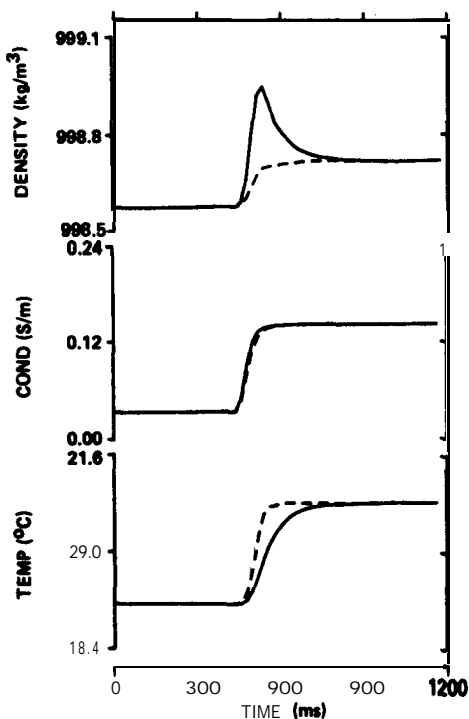


FIG. 12. Raw (solid line), and optimum (dashed line), step responses (Run 4). The temperature filter was 67/10, and the conductivity filter 0/15.

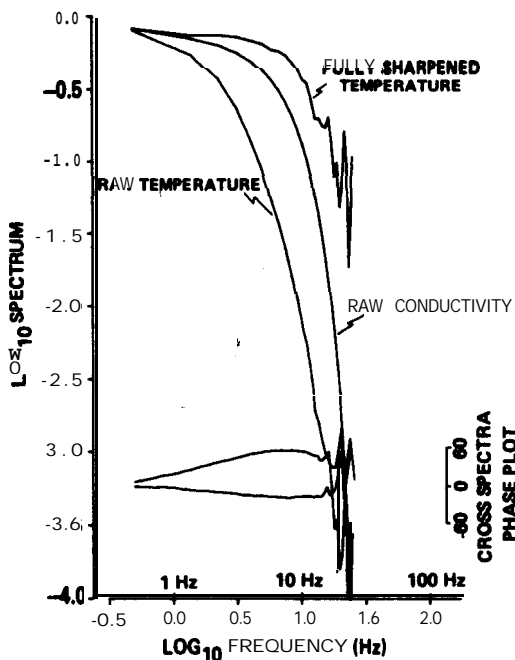


FIG. 13. Spectral plot of raw temperature, raw conductivity, and fully sharpened temperature, Run 4.

corresponds to a three-fold improvement in the temperature 3dB bandwidth, and demonstrates the ability of the technique to remove spiking in salinity and density by matching the sensor responses.

The high-frequency noise present in the spectra shown in Figs. 13 and 14 may be reduced by applying a third-order "brick-wall" filter; however, to demonstrate the noise amplification caused by the sharpening filter the low-pass filter has not been applied.

Note that the spectral plots were produced from the normalized sensor stepresponse multiplied by a Blackman-Harris window (Harris, 1978) before transformation with a 5 12-point fast Fourier transform (FFT). The spectral estimates were multiplied by the angular frequency ( $\omega$ ) to correct for the use of a step input rather than an impulse, and then squared to produce power spectral density. Finally, the 5 12 spectral points were averaged into 64 bins to improve the spectral estimates.

### 7. Application to a typical CTD cast

Much can be learned from a single CTD cast if the temperature and the conductivity are carefully matched and if the response is fast enough, at the given profile speeds, to resolve all significant finescale structures. The filtering described above is now routinely applied to all the CTD data which have a working resolution of about 20 ms or 0.02 m at a profiling speed of 1 m s<sup>-1</sup>. The need to define structures down to these scales has been identified by many workers (for a review see

Muller and Pujalet, 1984) and results mainly from the requirement to calculate the displacement scale of the motion. The displacement scale  $L$  (Thorpe, 1977) is the vertical distance a water particle has to be moved in order to produce a monotonically increasing density profile from the given measured profile. This distance is directly related to the Ozmidov length (Ozmidov, 1965) and the available potential energy of the water column (Dillon, 1984). When combined with the buoyancy frequency  $M$  from the monotonic density profile, a useful indicator  $M^3 L^2$  (m<sup>2</sup> s<sup>-3</sup>) of the dissipation of turbulent kinetic energy is obtained.

The results from a typical profile are shown in Fig. 15a, with an expansion of scales in Fig. 15b. The effect of the matching is clearly visible on all plots, and the influence on the displacement scale (Fig. 15a) and the dissipation estimate (Fig. 15a) is quite dramatic. In particular, for the step near 3.4 m, expanded in Fig. 15b, it is seen that the unstable spike in the raw density profile has been removed, resulting in a smooth two-step structure which appears to be the result of a small intrusion. On the other hand, the corrected signal was somewhat less stable near the 6 m mark. The signal there has a considerably larger displacement scale and therefore indicates a more active dissipation regime than that of the raw signal. The important point to note is that the matching of the sensors has led to considerable modification of the estimate of the dissipation, indicating the sensitivity of these estimators to any mismatch of the raw temperature and conductivity signals.

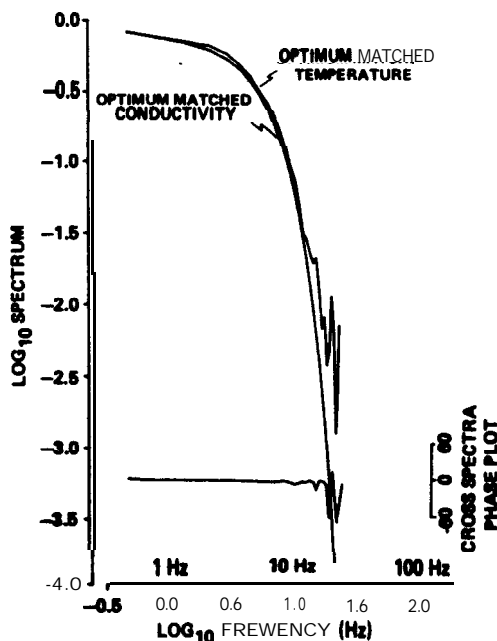


FIG. 14. Spectral plot of optimum matched responses of temperature and conductivity, Run 4. Note matching within 1 dB up to 15 Hz.

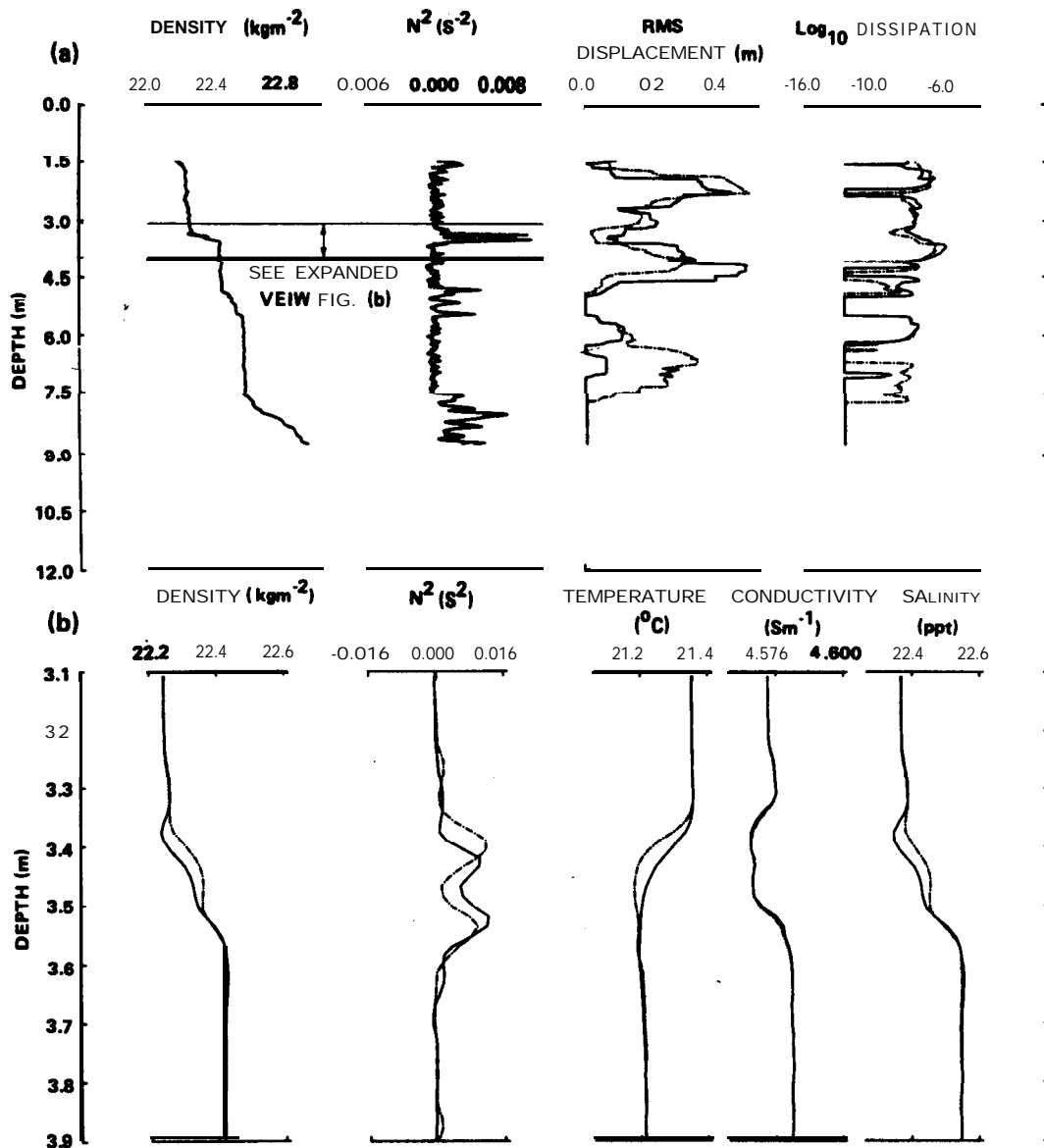


FIG. 15. (a) Example of a typical oceanic profile, raw (solid line), and corrected (dashed line) by this technique. (b) Expanded view of data in (a).

## 8. Summary and discussion

The sensor-response correction technique described in this report will be referred to as the recursive time-series technique. The SBE-3 temperature sensor has been modeled as a cascaded first-order system with three different time constants. It is hypothesized that these time constants correspond to the thermal effects of the fluid boundary layer (dependent on speed through the water), the thermal inertia of the protective metal shroud, and the thermal inertia of the glass thermistor bead. The time constants may be found in a number of ways, but the most accurate and direct

method is by plotting the natural logarithm of the normalized step response of the sensor. By modeling the sensor in this manner, the Z-transform yields a particularly elegant recursive technique for correcting the output of the sensor in the time domain. The technique has an identical effect to that of correcting the sensor spectrally, but the computation time is significantly reduced since it is not necessary to transform to and from the frequency domain.

The number of stages of correction necessary is determined by the requirements of the user. In the absence of noise it would be possible to correct the sensor response to perfection, but the upper practical limit is

determined by the loss of signal-to-noise ratio at high frequencies. It has been shown that it was possible to improve the 3dB cutoff frequency by a factor of about 7 with some noise amplification. However, the more conservative correction applied to the temperature sensor to match the conductivity sensor response (to within 1 dB up to 15 Hz) resulted in the improvement of the cutoff frequency by a factor of around 3. Note that this improvement resulted from the use of only a single correction time constant.

The use of a **time-domain** correction technique allows salinity and density to be calculated immediately. Moreover, the recursive nature of the technique described in this report allows high cutoff frequency, low-pass recursive filters to be implemented simultaneously to reduce noise outside the band of interest.

The main disadvantage of the recursive time series technique is that it may not be successfully applied to any arbitrary sensor. A sensor with a response that is not easily modeled as a cascaded first-order filter should not be corrected as such. The curve in the log-plot of the conductivity-sensor step response (Fig. 5) shows that this sensor is such a case. It may be legitimate to fit a straight line to the curve and derive one time constant, but to try to obtain several time constants would not be possible. In general, sensors with a poor response due to averaging or nonlinear effects (such as the **SBE-4** conductivity cell) are not good candidates for more than single time constant correction.

**Acknowledgments.** Michael **McGilvray** assisted with the experimental work, especially with regard to the implementation of the conductivity cell pump. David **Pullin** developed much of the software used for data processing, and George **Scolaro** helped with data **collection** software. **Geoff Carter** installed both fast response sensors into the experimental apparatus. This work was supported by the Australian Research Grants Scheme, Reference number F78 1566 1 R.

## REFERENCES

- Caldwell, D. R., and T. M. **Dillon**, 1981: An oceanic microstructure measuring system. School of Oceanography, Oregon State University, Ref. **81-10**, 168 pp.
- Dillon**, T. M., 1984: The **energetics** of overturning **structures: Implications** for the theory of fossil turbulence. *J. Phys. Oceanogr.*, **14**, 54-1549.
- Fofonoff**, N. P., S. P. Hayes and R. C. Millard, Jr., 1974: W.H.O.I./Brown CTD **microprofiler**: Methods of **calibration** and data handling. **WHOI Tech. Rep. WHOI-74-89**, 64 pp.
- Fozdar**, F. M., 1983: Mixed layer probe technical report. **Environmental Dynamics Report ED-83-039**, University of Western Australia. 68 pp.
- Gabel, R., and R. **Roberts**, 1973: *Signals and Linear Systems*. Wiley & Sons. **4** 15 pp.
- Gregg, M. C., and W. C. Hess, 1985: Dynamic response calibration of the Sea-Bird temperature and conductivity probes. *J. Atmos. Oceanic Technol.* **2**, 304-313.
- , and T. B. **Meagher**, 1980: The dynamic response of glass rod thermistors. *J. Geophys. Res.* **85**, 2779-2786.
- , J. C. Schedvin, W. C. Hess and T. B. **Meagher**, 1982: Dynamic response calibration of the Neil **Brown** conductivity cell. *J. Phys. Oceanogr.*, **12**, 720-742.
- Han-is, F. J., 1978: On the use of windows for harmonic analysis with the Discrete Fourier Transform. *Proc. IEEE*, **66**, 51-83.
- Head, M. J., 1983: The use of miniature four-electrode conductivity probes for high resolution measurement of turbulent density or temperature variations in **salt-stratified** water flows. Ph.D. thesis, University of California, 211 pp.
- Home, E. P. W., and J. M. **Toole**, 1980: Sensor response mismatches and **la8** correction techniques for temperature-salinity profilers. *J. Phys. Oceanogr.*, **10**, 122-130.
- Imberger**, J., 1985: The **diurnal** mixed layer. *Limnol. Oceanogr.*, **30**, 737-770.
- Muller**, P., and R. **Pujalet**, Eds., 1984: Internal Gravity Waves and **Small-Scale** Turbulence. *Proc. 'Aha Huliko'a Hawaiian Winter Workshop*, University of Hawaii at Manoa, Hawaii Inst. of Geophys. **Spec. Publ.**, 300 pp.
- Ozmidov**, R. V., 1965: On the turbulent exchange in a stably stratified ocean. *Atmos. Oceanic Phys.*, **1**, 493-497.
- Pederson**, A. M., and M. C. Gregg, 1979: Development of a small *in situ* conductivity instrument. *J. Oceanogr. Eng.* **4**, 69-75.
- Thorpe, S. A., 1977: Turbulence and **mixing** in a Scottish Loch. *Phil. Trans. Roy. Soc. London*. **A286**, 125-181.
- UNESCO, 1981: The practical salinity scale, 1978 and the **international** equation of state 1980. *Tenth report of the Joint Panel on Oceanographic Tables Standards*, UNESCO Tech. Paper in Mar. Sci. No. 36, 13-21.